INORGANIC CHEMISTRY FRONTIERS

RESEARCH ARTICLE

View Article Online
View Journal

Cite this: DOI: 10.1039/d5qi01858g

Tunable aurophilic aggregates as the basis of mechano- and thermochromism in gold(I) ethynyl complexes

Juan Carlos Pérez-Sánchez, [a] Jessica Cámara,[a] M. Carmen Blanco, [b] Lucía Aloras-Perún,[a] María Gil-Moles, [a] Rosa M. Gomila, [c] Antonio Frontera [c] and M. Concepción Gimeno *[a]

Mechanochromic materials that change colour in response to mechanical stimuli hold promise for applications in sensors, data storage, and smart materials. Here we report the mechanochromic and thermochromic behaviour of a systematic isostructural series of gold(I) ethynyl–pyridine complexes, where the position of the pyridine nitrogen atom is varied and compared to a phenyl analogue. All compounds display striking luminescence changes upon mechanical grinding and thermal treatment, with emission consistently shifting to a common green state (520–540 nm). These transformations are reversible upon solvent-vapour exposure and are also retained in PMMA films. Structural (PXRD) and photophysical analyses reveal that these spectral shifts arise from packing-dependent modulation of two accessible excited-state manifolds: a higher-energy ILCT state and a lower-energy state whose stabilization is highly sensitive to aurophilic aggregation and local microstructure. Mechanical grinding disrupts long-range order and generates disordered microdomains that favour this aggregated CT-type excited state and enhance its radiative efficiency, contributing to the strong green mechanochromism. These results demonstrate how subtle ligand variations can direct supramolecular packing and excited-state balance to achieve robust, reversible chromic responses, providing general design principles for next-generation stimuli-responsive Au(I) luminescent materials.

Received 9th September 2025,
Accepted 28th November 2025

DOI: 10.1039/d5qi01858g

rsc.li/frontiers-inorganic

Introduction

Mechanochromic materials, compounds that change colour in response to mechanical stimuli, have attracted significant attention due to their potential in diverse applications, such as sensors,[1] data storage,[2] or smart materials.[3] These colour-changing properties arise from alterations in the molecular structure, intermolecular interactions, and crystalline packing when subjected to pressure or shear force.[4,5] In this context, metal complexes offer a modular platform for tuning photophysical responses through both ligand design and supramolecular assemblies.[6–10] Among them, gold(I) complexes stand out,[11–13] due to their high spin–orbit coupling constant (ζ = 5100 cm^{-1}),[14] propensity for aurophilic (Au···Au) interactions,[15–19] and linear coordination geometry, which collectively facilitate triplet-state phosphorescence and solid-state self-organization. Among these complexes, gold(I) alkynyl complexes are attractive for their low-energy π–π^*(C≡CR) transitions and charge transfer transitions between the alkynyl ligand and the metal center (Fig. 1a).[20–25] Moreover, their two-coordinate linear geometry promotes the formation of supramolecular aggregation *via* Au···Au interactions,[26] which can be modulated through subtle ligand changes.[20] Although a handful of alkynyl-based gold(I) systems exhibiting mechanochromic behavior have been reported,[20,27–29] these remain isolated examples, and the field continues to be dominated by studies on gold(I) isocyanide analogues.[30,31] Given the geometric and electronic similarity between the alkynyl and isocyanide groups, gold(I) alkynyl complexes remain an underexplored yet promising scaffold for stimuli-responsive materials.

Within this framework, pyridine-based alkynyl ligands offer an appealing strategy to modulate electronic distribution and intermolecular interactions. Their π-deficient character and significant dipole moments enhance conjugation and π-stacking potential, thereby influencing both supramolecular packing and the photophysical response.[32–36] Subtle structural

[a]Departamento de Química Inorgánica, Instituto de Síntesis Química y Catálisis Homogénea (ISQCH), CSIC-Universidad de Zaragoza, 50009 Zaragoza, Spain. E-mail: gimeno@unizar.es
[b]Centro Universitario de la Defensa, Universidad de Zaragoza-Academia General Militar, 50090 Zaragoza, Spain
[c]Departament de Química, Universitat de les Illes Balears, Crta de Valldemossa km 7.5, 07122 Palma de Mallorca, Baleares, Spain

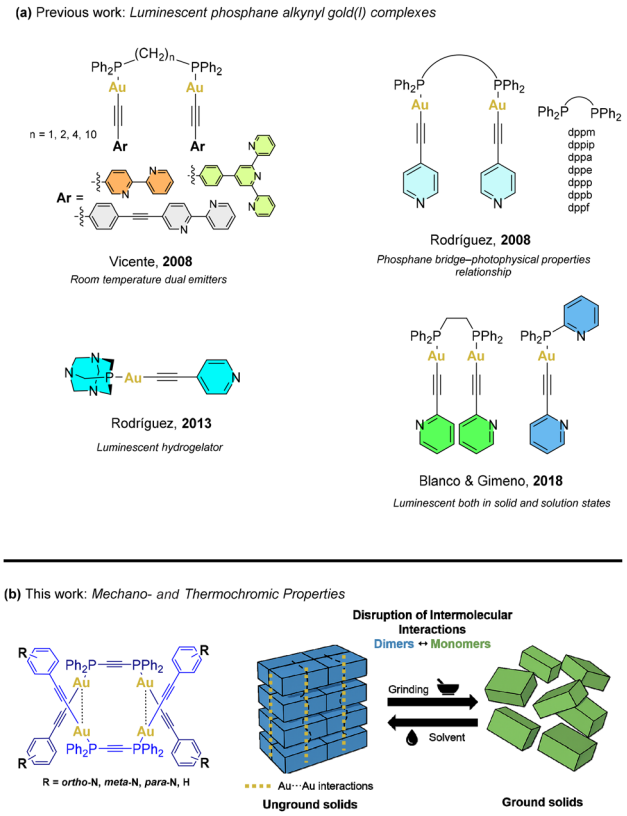

Fig. 1 (a) Previous examples of gold(I) phosphane–alkynylpyridine compounds with luminescence properties.[24,32,33,35] (b) This work and schematic depiction of the mechanochromism process, showing the structural changes of the molecular packing when a mechanical stress is applied over a compound.

variations, such as the position of the nitrogen atom on the pyridine ring, can profoundly affect Au···Au contacts and crystal packing, offering a rational route to control mechanoresponsive behaviour.

In most known Au(I) mechanochromic systems, mechanical grinding typically induces a red shift associated with the strengthening of aurophilic contacts.[37–39] In contrast, our study reveals a distinct and counterintuitive mechanism: grinding triggers a bathochromic shift not through enhanced Au···Au contacts, but *via* a packing-driven reorganization of the aurophilic assemblies into a disordered emissive state with a different emissive character. This behaviour underscores the critical, yet often overlooked, role of supramolecular packing beyond simple Au···Au distance correlations.

Despite significant progress, previous research has largely centered on individual compounds or families interpreted through simplified structure–emission relationships. Systematic investigations unravelling the interplay of packing, aurophilicity, and emission behavior remain scarce. Moreover, dual mechano- and thermochromism, as well as the incorporation of such responsive systems into polymer matrices, have received limited attention, despite their importance for functional applications.

In this contribution, we present a comprehensive study of an isostructural series of pyridyl–ethynyl gold(I) complexes (**6–9**), all of which exhibit reversible dual mechano- and thermochromism. Mechanical grinding or embedding in PMMA consistently drives the emission to a common green state (520–540 nm), which can be restored to the original color by solvent-vapor annealing. Combined PXRD, luminescence, and DFT analyses reveal that the optical transformations arise from a packing-controlled reorganization of aurophilic aggregates rather than direct modulation of Au···Au distances. By elucidating this mechanism and establishing structure–response correlations across a controlled series, this work introduces new design principles for Au(I) alkynyl mechanochromic materials and demonstrates a generalizable route toward tunable, stimuli-responsive luminescence.

Results and discussion

Synthesis and characterization

Firstly, all synthesized complexes share a common preparation route: the reaction of a gold(I)-alkynyl polymer with a dppa ligand. These polymeric complexes are readily obtained by treating the respective alkynyl derivative (R = **2-py**, **3-py**, **4-py** and **Ph**) with [AuCl(tht)] in dichloromethane using a 1 : 1 molar ratio and NEt_3, leading to the immediate precipitation of the gold(I) complexes **2–5** (Scheme 1). These polymers are obtained as air stable yellow to green solids, insoluble in most solvents.[40] Subsequent treatment of these intermediates with dppa **1** in a 1 : 2 molar ratio results in the formation of complexes **6–9** (Scheme 1).

The ^{1}H NMR spectra of complexes **6–9** display the expected signals for the aromatic protons of both the phosphane and aryl ligands (see the SI). The $^{31}P\{^1H\}$ NMR spectra display broad singlets at δ_P ranging from 10.5 to 15.6 ppm representing a substantial downfield shift from free dppa (δ_P = −32.5 ppm).[41] Notably, the full width at half maximum ($\Delta\nu_{1/2}$) of the $^{31}P\{^1H\}$ peaks is notably broadened across the series

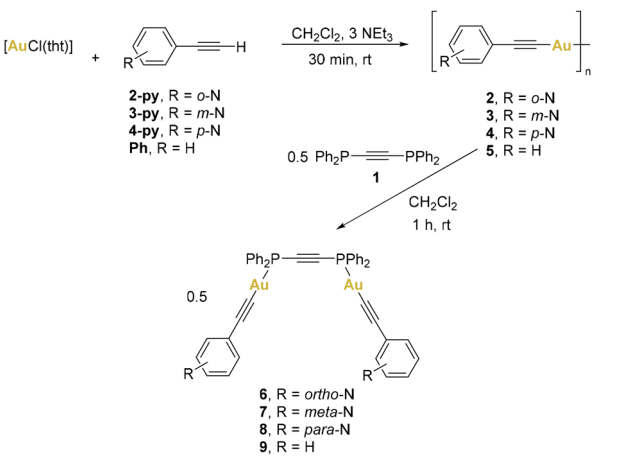

Scheme 1 Synthesis of dppa gold(I) complexes **6–9**.

($\Delta\nu_{1/2}$ = 52–446 Hz), suggesting dynamic exchange between coordination environments, particularly between the monomeric and dimeric forms.[42] IR spectroscopy further confirms the presence of both alkynyl fragments, with ν(C≡C) bands consistently observed around 2100 cm^{-1}. Single-crystal X-ray diffraction analysis reveals that complexes **6–9** adopt dimeric structures in the solid state, stabilized by intermolecular aurophilic contacts with Au···Au distances ranging from 2.9932(4) to 3.0735(3) Å (Fig. 2a). However, the geometry of the dimeric units differs across the series. Complexes **6** and **9** exhibit an orthogonal arrangement of monomeric units, with the diphosphane ligands oriented nearly perpendicular to each other. In contrast, complexes **7** and **8** display an offset face-to-face geometry, characterized by a laterally shifted π-stacking of the monomers. These differences in dimer orientation translate into distinct crystal packing motifs, where **6** and **9** share an identical arrangement, distinct from the common packing observed for **7** and **8** (Fig. 2b). The packing architectures are further stabilized by weak non-covalent interactions. Moreover CH···π contacts involving the alkyne or phenyl π systems are observed in all structures, while complex **8** also features CH···N interactions involving the pyridyl nitrogen, and **9** lacks these interactions. Notably, **8** crystallizes in a space group ($P2_1/c$) different from that reported for the same species ($P\bar{1}$) by Ferrer *et al.* and exhibits distinct luminescence. We ascribe this to polymorphism, whereby altered crystallization conditions afford an alternative packing motif (offset face-to-face dimers with Au···Au contacts and CH···N interactions) that modulates the emissive properties. The PXRD results of the bulk material match the simulated pattern from our SC-XRD model, confirming the phase purity of this polymorph and rationalizing the photophysical differences observed. These supramolecular interactions, along with the dimer geometry, define the extended packing and are consistent with the observed mechanochromic response.

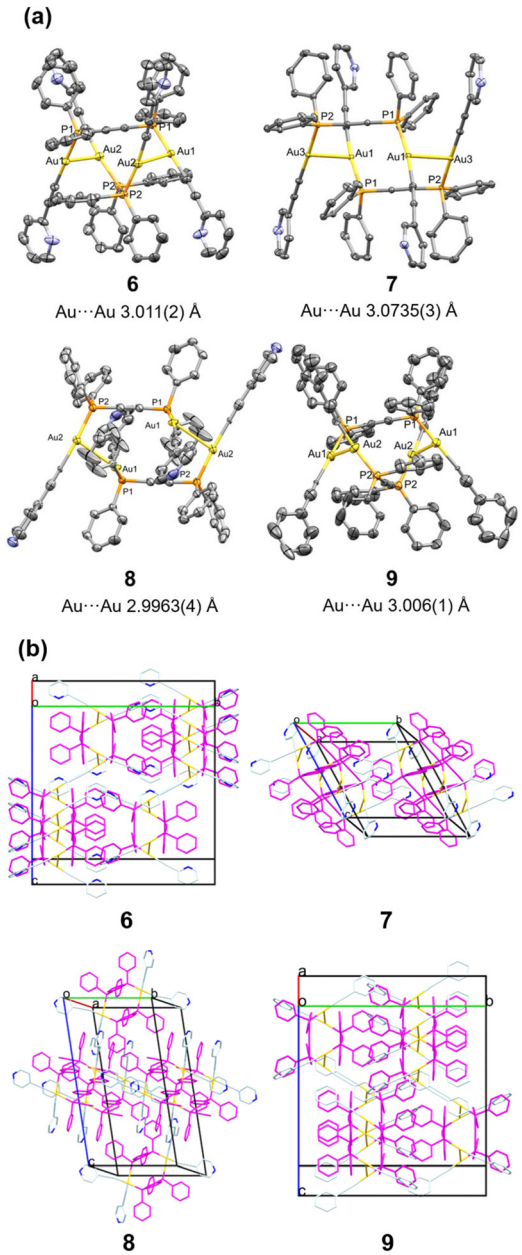

Fig. 2 (a) Single crystal X-ray diffraction showing the molecular structures of complexes **6–9**; yellow: gold, orange: phosphorus, blue: nitrogen, grey: carbon (50% displacement ellipsoids, hydrogen atoms have been omitted for clarity). (b) 3D crystal packing of complexes **6–9** viewed along the *a**-axis; yellow: gold, light blue: ethynyl fragment, blue: nitrogen, magenta: dppa fragment.

Additional geometrical parameters are listed in Table S9 and are in good agreement with this type of structure.[32] The structural divergence among dimers correlates with the differences observed in photophysical behaviour, providing a solid basis for interpreting the origin of the luminescent response as a function of packing and Au···Au interaction geometry. Thermogravimetric analysis (TGA) of complexes **6–9** reveals initial weight losses below 5% near 100 °C (Fig. S26–S33), consistent with the release of approximately two equivalents of adsorbed water per formula unit. At elevated temperatures, distinct decomposition events are observed. Complexes **6** and **8** display an initial mass loss of ~10% with T_{onset} values at 289 °C and 262 °C, respectively, attributable to the elimination of one ethynylpyridine moiety. Above 350 °C, all complexes undergo major weight loss, ascribed to the decomposition of the dppa backbone, leading to residual gold-containing species. Notably, ground samples exhibit T_{onset} values for the main decomposition event approximately 10 °C higher than those of their pristine counterparts, indicating enhanced thermal stability. This shift suggests a mechanically induced phase transformation, likely accompanied by rearrangement of molecular packing or modification of intermolecular contacts.

Photophysical properties: mechano- and thermochromism

A mechanochromic response was first observed serendipitously for complex **6**, where scratched areas displayed green–yellow luminescence under UV light (λ = 365 nm), contrasting with the weak blue emission of the pristine solid. This led to a systematic evaluation of the luminescence properties of complexes **6–9** under mechanical stimulation, confirming mechan-

oresponsive behaviour across the series (Fig. 3), likely arising from a crystal-to-amorphous or crystal-to-crystal phase transition induced by shear force.[11] Thus, to gain further insights into potential structural changes upon mechanical stimulation, powder X-ray diffraction (PXRD) analyses were conducted on both pristine and ground samples of each compound (Fig. 3). For clarity, "pristine (unground) powder" denotes the bulk microcrystalline powder as isolated and packed without intentional grinding; "ground powder" refers to the same material after manual grinding with an agate mortar. Mechanical grinding induced notable changes in the PXRD patterns of all four complexes, including attenuation and broadening of reflections and, in some cases, the disappearance of characteristic peaks, indicating partial loss of long-range order and formation of an amorphous phase. Among the series, **9** showed the highest residual crystallinity, suggesting that its molecular packing resists amorphization more effectively. To assess the reversibility of this structural disruption, the ground powders were exposed to CH_2Cl_2 vapor. PXRD analysis revealed almost complete recovery of the initial diffraction patterns, with the reappearance of key reflections and sharpening of peaks, consistent with recrystallization. This reversible structural transformation correlates with the luminescence behaviour: grinding disrupts the ordered arrangement, including Au–Au contacts, modifying emission properties, while vapor exposure promotes partial restoration of the original packing and emission profile. These results confirm that the mechanochromism arises from a reversible solid-state phase transition governed by changes in the intermolecular organization of the dimers formed within the pristine solids.[43] In addition, Raman spectroscopy provides an independent probe of the structural changes induced by mechanical stimulation. For complex **7**, the alkynyl stretching region, ν(C≡C) ≈ 2100–2130 cm^{-1}, shows a marked decrease in band intensity in the ground powders relative to the pristine microcrystalline solids (Fig. S14B). This attenuation is consistent with a loss of long-range order, increased microstructural heterogeneity, and a greater degree of orientation averaging of the Raman tensor, likely arising from partial reorientation or distortion of the alkynyl fragments upon grinding.[44] Taken together with PXRD data, these Raman trends support a scenario in which mechanical grinding disrupts the crystalline registry yet creates locally aggregated/disordered domains where effective aurophilic proximity is maintained or reinforced.

In their pristine form, all complexes exhibit emission in the blue region. The excitation spectra show broad, vibronically unresolved bands between 250 and 365 nm, with excitation maxima ranging from 330 to 365 nm. At room temperature, the emission maxima are located between 377 nm and 426 nm (Fig. 4a). Lifetime measurements reveal notable differences, with average values ranging from 12.2 μs (**9**) to 296.4 μs (**7**), while the photoluminescence quantum yields (PLQYs) are modest (≤4.6, in case of **9**) Upon cooling to 77 K, excitation spectra shift toward higher energies, typically by 20–30 nm (Fig. S35). The emission spectra undergo slight blue shifts and, in some cases, display increased vibronic resolution (Fig. S35), attributed to the ground-state phenyl ring deformations and C≡C stretching frequencies (Table 1).[45]

These results point to significant temperature-dependent modulation of the photoluminescence properties. When

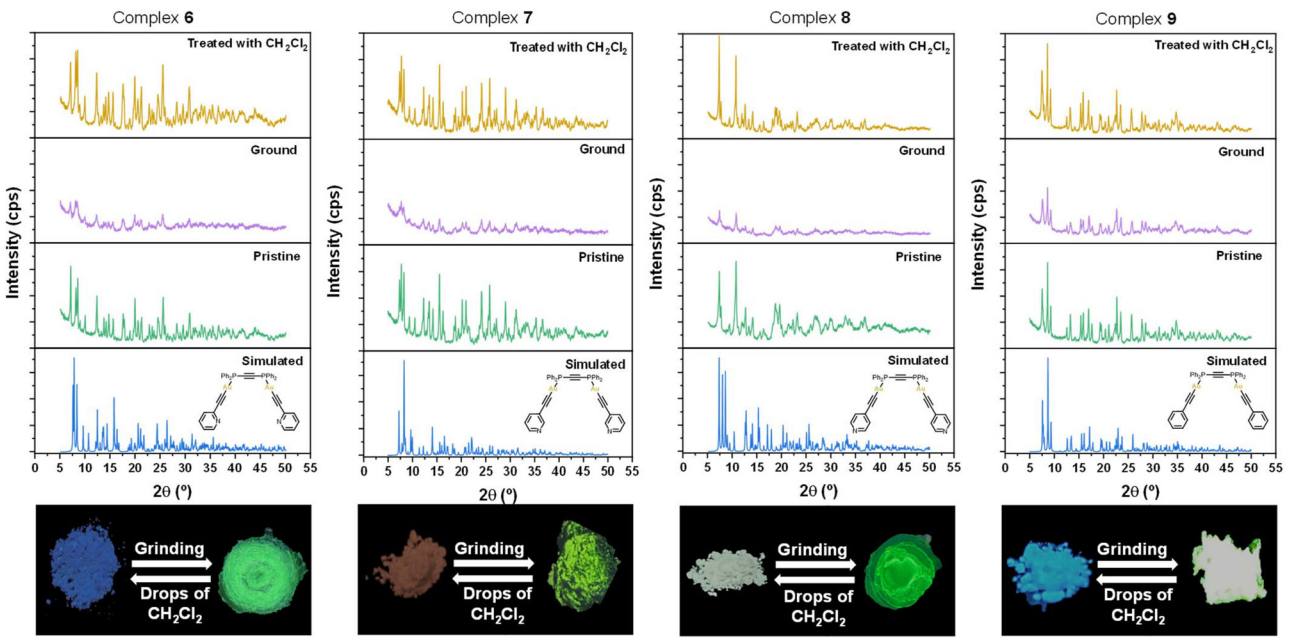

Fig. 3 PXRD patterns of complexes **6–9**, simulated pattern from the XRD structure (blue), experimental pattern of the pristine powder (green), experimental pattern of the ground powder (violet), experimental pattern of the ground powder after addition of drops of CH_2Cl_2 (yellow) and photographs of the powders showing their reversible behaviour.

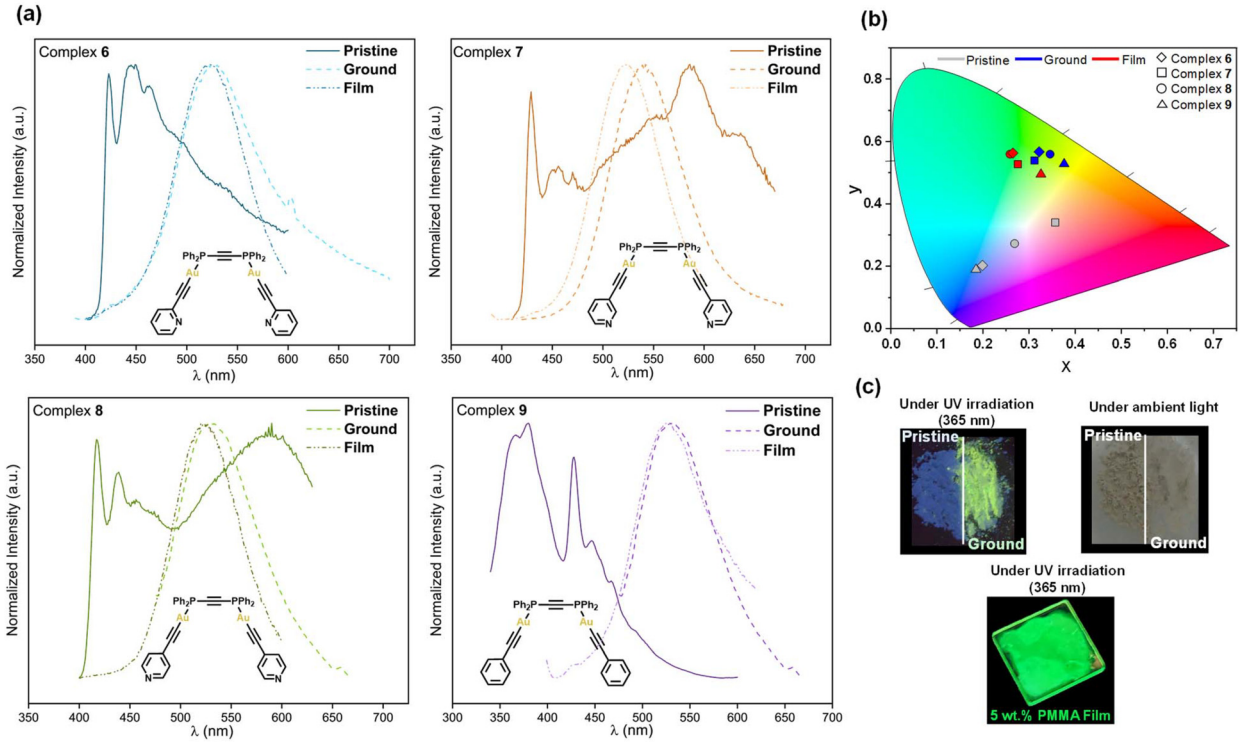

Fig. 4 (a) Emission spectra of complexes **6–9** as pristine solids at room temperature. (b) CIE chromaticity diagram (CIE 1931) showing emission colour variance for pristine, ground solids and PMMA (5% w/w) films of **6–9**. (c) Photographs of compound **6** upon scratching the right half, under 365 nm UV light (up left), under room light (up right) and compound **6** as a PMMA film under 365 nm UV light (bottom center).

Table 1 Photoluminescence data for complexes **6–9** as solid powders in pristine, ground and film forms

	Pristine solids					Ground solids					PMMA films				
Complex	T^a	$\lambda_{ex}{}^b$	$\lambda_{em}{}^b$	$\tau_{av}{}^c$	$\Phi_{PL}{}^d$	T^a	$\lambda_{ex}{}^b$	$\lambda_{em}{}^b$	$\tau_{av}{}^c$	$\Phi_{PL}{}^d$	T^a	$\lambda_{ex}{}^b$	$\lambda_{em}{}^b$	$\tau_{av}{}^c$	$\Phi_{PL}{}^d$
6	rt	365	422	42.3	<1	rt	400	535	960	1.0	rt	380	520	1.7	4.4
	77	314	436	34 850	n.d.	77	370	520	32 900	n.d.					
7	rt	347	426, 586	296.4	1.0	rt	400	540	158	6.0	rt	380	520	1.1	7.7
	77	340	436, 526	30 000	n.d.	77	335	525	4210	n.d.					
8	rt	340	420, 585	95.8	2.1	rt	400	530	133.8	7.7	rt	380	520	1.2	9.0
	77	334	416, 528	13.2	n.d.	77	380	525	10.7	n.d.					
9	rt	330	377	12.2	4.6	rt	413	5.2	11.6	5.6	rt	385	520	11.1	3.1
	77	343	426	16.6	n.d.	77	375	530	15.1	n.d.					

[a] T, temperature (in K), rt, room temperature (293 K). [b] λ_{ex}, excitation maxima (in nm), λ_{em}, emission maxima (in nm). [c] Lifetime average values (in μs) fitted to a double or triple exponential equation (see the SI). [d] Photoluminescence quantum yield at room temperature (in %). n.d., not determined.

ground, the emission spectra of **6–9** shift markedly toward lower energy (Fig. 4a), with new unstructured bands appearing around 530–540 nm (Fig. S34) resulting in a yellow–green emission (Fig. 4b and c). Excitation maxima also red-shift to 370–413 nm. This bathochromic shift observed upon grinding reflects changes in molecular packing. Since Au···Au interactions govern the formation of self-assembled dimers in the solid state for the entire series of complexes, we hypothesize that the observed shift arises from a change of these interactions. This possibility is further explored in the theoretical analysis presented below. Notably, similar behaviour has been previously reported for gold clusters with strong Au(I)···Au(I) interactions,[46] in which grinding-induced bathochromic shifts were attributed to transitions from crystalline to amorphous phases, resulting in altered aurophilic contacts. These spectral changes are accompanied by a pronounced increase in both emission lifetimes and PLQYs. The highest efficiency is observed for $\mathbf{8}_{\mathbf{ground}}$, while $\mathbf{9}_{\mathbf{ground}}$, although less affected in

lifetime (11.6 μs), reaches a PLQY of 5.6%. At 77 K, all ground samples show further lifetime enhancement, with emission maxima around 520–530 nm (Fig. S35). Variable temperature measurements ($\mathbf{6}_{\mathbf{ground}}$ and $\mathbf{9}_{\mathbf{ground}}$) had minimal impact on emission wavelength but induced hypsochromic shifts in excitation (~20–30 nm, Fig. S37).

To clarify the origin of the intricate luminescence patterns in this family, we concentrated our efforts on complex **7**. While compounds **6** and **9** show a straightforward single-band emission in the pristine solid (although with a long tail), complexes **7** and **8** display a characteristic dual emission, immediately suggesting the coexistence of two emissive species or excited states. In the pristine solid state, **7** exhibits two bands at *ca.* 426 and 586 nm (436 and 526 nm at 77 K), consistent with a higher-energy ILCT-type state that is weakly sensitive to packing, and a lower-energy, environment-dependent charge transfer state stabilized by the aurophilic contacts present in the offset dimers. The markedly larger temperature dependence of the latter (586 → 526 nm) supports its attribution to an excited state strongly perturbed by metallophilic coupling and lattice relaxation. This dual behavior is mirrored in solution: at high concentration, **7** shows two emissions at *ca.* 415 and 545 nm, closely resembling the solid-state pattern (Fig. S44). The disappearance of the 545 nm band upon dilution confirms that this lower-energy component originates from emissive aggregates or transient dimers that retain Au···Au interactions, whereas the higher-energy band around 385–415 nm persists in all environments and therefore represents an intrinsic ILCT excited state accessible to both monomeric and aggregated species.

The behavior of **7** under mechanical stimulation is fully coherent with this assignment. Upon grinding, the low-energy emission shifts to *ca.* 520 nm and becomes significantly more intense. This response is best rationalized by recognizing that grinding disrupts the long-range crystalline order while generating numerous locally aggregated, disordered microdomains in which short Au···Au contacts are maintained or newly formed. These microenvironments stabilize the same aurophilically perturbed CT transition responsible for the 586 nm (pristine solid) and 545 nm (concentrated solution) bands, but with reduced structural relaxation and slightly weakened CT stabilization, leading to the observed blue-shift to 520 nm. At the same time, the mechanical disruption restricts intramolecular motions and suppresses nonradiative decay, increasing both the population and radiative efficiency of the emissive aggregates. As a result, the 520 nm band becomes the dominant emissive channel in the ground sample. Altogether, the evolution 586 → 545 → 520 nm across pristine solid, concentrated solution, and ground material reflects the progressive modulation of Au···Au interactions and CT stabilization, which contribute to the dual emission and mechanochromic behaviour of complex **7**. A similar rationalization can be extended to complexes **6** and **9**, although in these systems the low-energy, aurophilically perturbed CT emission is much weaker, almost negligible, in their pristine solids, indicating that their crystal packing either disfavors or only minimally stabilizes the emissive aggregated states that dominate in **7** and **8**.

To further probe the impact of disrupted packing, complexes **6–9** were embedded in PMMA films (5 wt%), with emission profiles closely resembling those of the ground powders (Fig. 4a–c and S36), with maxima at *ca.* 520 nm. While PMMA films exhibit shorter lifetimes than ground solids, their quantum yields are comparable or even higher, up to 9.0% for $\mathbf{8}_{\mathbf{film}}$. Notably, grinding enhances PLQYs across the series, with up to six-fold increases for $\mathbf{6}_{\mathbf{ground}}$ and $\mathbf{7}_{\mathbf{ground}}$. A high variability in lifetime data was found between batches, and it likely reflects microstructural inhomogeneities (*e.g.*, amorphous/crystalline domains, aggregation and monomer/dimer ratios). These trends map onto two packing families: orthogonal dimers (**6** and **9**, $C2/c$ space groups) and offset face-to-face dimers (**7** and **8**, $P\bar{1}$ and $P2_1/c$ space groups, respectively) and correlate with the photophysical properties: **7** and **8** show dual emission and more facile loss of long-range order upon grinding, whereas **9** exhibits a smaller lifetime gain. Time-resolved data and PXRD thus indicate that pyridyl *ortho*, *meta* and *para* substitution tunes the dimer/monomer ratio and packing rigidity, which controls the threshold and magnitude of mechanochromic response.

To further understand how these complexes behave in solution, we selected **6** for detailed photophysical analysis. In CH_2Cl_2 at 298 K, it displays structured emission at ~450 nm. Upon cooling to 77 K, a broader, unstructured band emerges at 500 nm. Notably, an intermediate yellow emission (~550 nm) appears under UV excitation at temperatures between 298 and 77 K, indicating thermochromic luminescence (Fig. 5).[47] Emission spectra were recorded across a range of temperatures for compound **6** (Fig. 5a, S38–S40 and Tables S1, S2). The recorded data for the excitation and emission maxima reveal four distinct transitions at 380, 450, 550, and 500 nm.

The yellow band (550 nm) grows below 216 K and is replaced by the blue band (500 nm) below *ca.* 136 K. Notably, this hypsochromic shift was absent for complex **6** in the pristine form when the emission profiles were recorded at varying temperatures (Fig. S37a). This sequential emission shift is reversible and solvent-independent, occurring similarly in acetone and THF. For **9**, analogous behaviour is observed, although the transitions occur at slightly higher temperatures (Tables S2 and S4).

These bands never appear simultaneously, but intermediate emissions were observed at certain temperatures. Both emissions exhibit similar profiles and nearly identical excitation spectra, suggesting a shared excited state. Since the 550 nm band emerges above the freezing points of the solvents (178–165 K), molecular aggregation is likely initiated before complete freezing, leading to aurophilic interactions between solute molecules. Analogous behaviour has been reported in gold carbene complexes, where aurophilic aggregation in frozen media triggers new emission bands.[48] In our case, the gradual hypsochromic shift from 550 to 500 nm is consistent with rigidochromism: as the matrix becomes more rigid upon

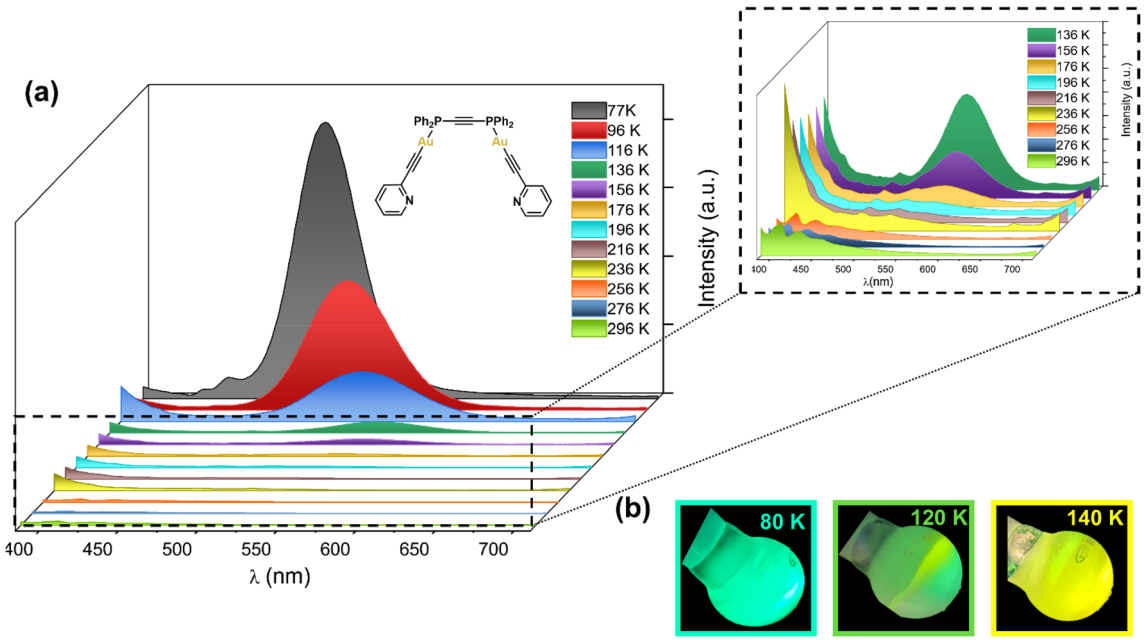

Fig. 5 (a) Emission spectra (λ_{ex} = 365 nm) of complex **6**, in CH_2Cl_2, (5×10^{-4} M) at different temperatures and details of these emissions in the range of 296–136 K. (b) More intense emissions of complex **6**: 550 nm emission band (yellow) and 500 nm emission band (blue); temperatures are illustrative.

cooling, solvent reorientation around the excited-state dipole is hindered, leading to emission from a less stabilized excited state.[49–51] This thermochromic behaviour was found to be fully reversible upon repeated cycles of freezing–warming.

Theoretical calculations

The photophysical properties of the Au···Au dimers of compounds **6** and **9** were investigated. The excitation to the S_1 state originates mainly from the H → L transition (90% for **6** and 93% for **9**). The higher excited states (S_2–S_8) exhibit nearly zero oscillator strength ($f \leq 0.07$) and therefore contribute minimally to the absorption spectrum (Table 2).

The calculated S_1–T_1 energy gaps for compounds **6** and **9** are 0.75 eV and 0.63 eV, respectively. These relatively small energy splittings promote intersystem crossing (ISC) by enhancing the spin–orbit coupling efficiency.

Consequently, ISC is moderately favoured in both systems, with compound **9** exhibiting a slightly stronger driving force due to its narrower gap. The $S_0 \leftarrow T_1$ vertical emission energies are 2.43 eV and 2.45 eV for **6** and **9**, corresponding to wavelengths of 510 nm and 506 nm, respectively. Inspection of the Natural Transition Orbitals (NTOs, see Fig. 6) confirms a transition dominated by an intraligand charge transfer (ILCT, π–π*) character, with significant involvement of the C≡C triple bond and the aromatic ring. Furthermore, a minor metal-to-ligand charge transfer (MLCT) character is also observed, as the hole orbital exhibits a small contribution from the d-orbitals of the Au(I) metal centers.

Thus, the transition is essentially ligand based but metallophilically perturbed. Hence, we then evaluated the role of aurophilic interactions in modulating the emissive properties of the complexes, using compounds **6** and **9** as representative models. To assess the strength of these interactions, we employed a literature-based approach that estimates interaction energies from the electron density (ρ) at the bond critical point (BCP) of the Au···Au contact: E (kcal mol^{-1}) = $-688.65 \times \rho$ (a.u.) + 10.03.[52] QTAIM analyses (Fig. 7) confirm the presence of BCPs and bond paths between the Au atoms in

Table 2 TD-DFT study of the dimers of compounds **6** and **9** at the B3LYP-D4/def2-TZVP level of theory

Complex	Trans.	Comp.	λ_{abs}	f	S_1–S_0	S_1–T_1	S_0–T_1
6	$S_0 \rightarrow S_1$	H → L (90%) ILCT$_{major}$ & MLCT$_{minor}$	343	0.169	3.61	0.75	2.86
9	$S_0 \rightarrow S_1$	H → L (93%) ILCT$_{major}$ & MLCT$_{minor}$	356	0.187	3.48	0.63	2.85

Absorption wavelength (λ_{abs}) and energies for $S_0 \rightarrow S_1$, S_1–T_1, and the vertical T_1 energy (S_0–T_1) are given in eV. Oscillator strength (f) and orbital composition (only contributions > 5% are indicated). The S_0–T_1 values represent the vertical transition energy, whereas the emission energies discussed in the text (2.43 and 2.45 eV) correspond to the $S_0 \leftarrow T_1$ vertical emission from the optimized T_1 geometry.

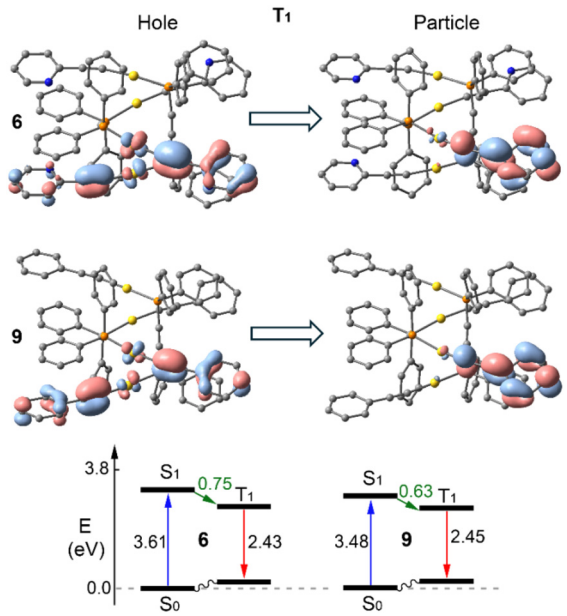

Fig. 6 (Top/middle) Natural transition orbitals (NTOs) to the first triplet transitions of the dimers of compounds **6** and **9**, respectively. (Bottom) Schematic energy level diagram calculated at the TD-DFT/B3LYP-D4/def2-TZVP level.

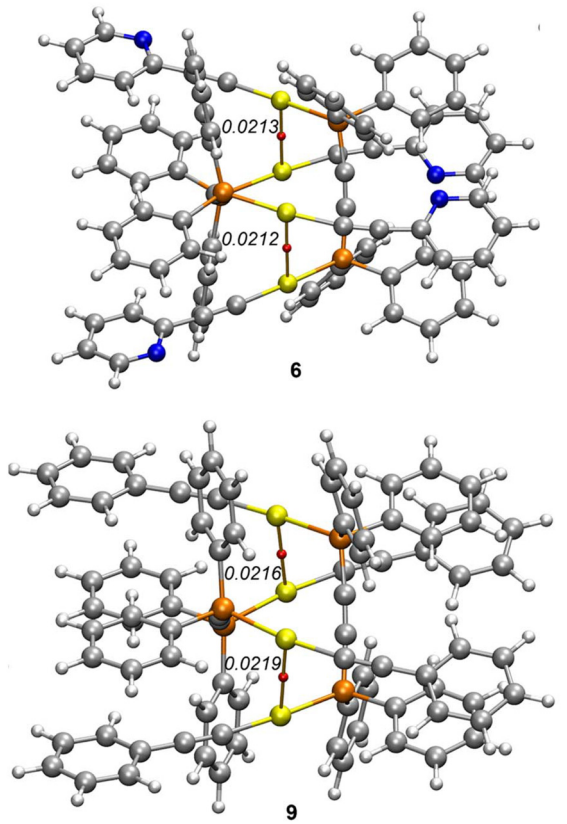

Fig. 7 QTAIM analysis of the dimers of **6** (top) and **9** (botton). Only the bond critical points (BCPs, small red spheres) connecting the Au-atoms are shown for clarity. The density values at the BCPs are given in a.u.

the dimers of **6** and **9**, yielding estimated aurophilic interaction energies of −4.7 and −5.2 kcal mol^{-1}, respectively.

Furthermore, we computed the phosphorescence emission wavelengths of monomeric models of compounds **6** and **9** that lack aurophilic contacts. As a result, we observed hypsochromic shifts of 12.5 nm and 17.6 nm with respect to the dimers for **6** and **9**, respectively. This supports the hypothesis that changes in molecular packing caused by mechanical grinding, likely due to altered Au···Au and π-stacking interactions in the solid state, affect the energy gap between the excited and ground states. Briefly, when the conjugation within the complex remains unaltered, the emissions are primarily attributed to ILCT transitions. However, upon grinding, the molecular packing and long-range order of the crystal are disrupted, leading to changes in the electronic structure that extend beyond the influence of the ligands alone. This mechanical stimulus could facilitate the formation of new aurophilic (Au···Au) interactions, indicating a more pronounced participation of the gold centers in the excited-state transitions. As a result, the emission may no longer be dominated by simple ILCT transitions but instead involve significant contributions from the gold atoms. This structural change apparently led to the deactivation of a non-radiative decay pathway present in the pristine solid, causing the observed increase in the measured PLQYs. The additional CH···N contacts in **8** and the absence of N in **9** rationalize their distinct packing resilience, PXRD evolution, and quantum-yield trends, underscoring positional isomerism as an effective lever to program packing-dependent luminescence.

Conclusions

In summary, this study demonstrates that subtle ligand and positional modifications in gold(I) ethynyl–pyridine complexes provide powerful control over supramolecular organization and, consequently, their mechano- and thermochromic responses. Across the series, luminescence arises from two accessible excited-state manifolds: a higher-energy ILCT-type state and a lower-energy state whose energy and efficiency are highly sensitive to aurophilic aggregation and local microstructure. The relative population and stabilization of these states depend strongly on crystal packing, the extent of metallophilic interactions, and the rigidity of the surrounding environment.

Mechanical grinding induces pronounced chromic shifts by disrupting long-range order and generating numerous locally aggregated, disordered microdomains in which short Au···Au contacts persist or are newly formed. These microenvironments favor the lower-energy CT transition emissive state and simultaneously restrict intramolecular motions, leading to enhanced emission intensity and the characteristic green mechanochromism. The process is fully reversible: solvent-vapor annealing restores the original packing arrangement and selectively re-establishes the higher-energy emissive pathway.

Thermal stimuli operate through a related mechanism, where lattice rigidification, altered packing relaxation, and

changes in the local dielectric environment modulate the energetic balance between the two emissive states, giving rise to distinct thermochromic behavior. Positional isomerism in the pyridyl ligands further tunes packing rigidity, aurophilic alignment, and aggregation propensity, enabling predictable control over chromic thresholds, emission efficiency, and solid-state sensitivity.

Overall, this work offers a unified structure–property framework linking aurophilic assembly, supramolecular packing, and excited-state modulation in gold(I) alkynyl systems. The demonstrated reversibility, dual-state emission, and robust chromic responses highlight these complexes as promising candidates for stimuli-responsive luminescent materials, reversible optical memory, and adaptive photonic devices.

Author contributions

J. C. P.-S. and J. C. contributed equally. J. C. P.-S, J. C., L. A.-P. and M. G.-M. synthesized, analysed, characterized and performed the photophysical measurements of all compounds. M. C. G. and M. C. B. designed the project and supervised the experiments. R. M. G. and A. F. performed the theoretical study and contributed to the writing of the DFT part. The draft manuscript was written by J. C. P.-S., J. C. and M. C. G., and all the authors finalized the manuscript through proofreading. All authors approved the final version of the manuscript.

Conflicts of interest

There are no conflicts to declare.

Data availability

The data supporting this article have been included as part of the supplementary information (SI). Supplementary information: experimental details, NMR spectra, TGA data, additional emission and excitation spectra, lifetime fitting curves, crystallographic data, computational details and additional figures and tables. See DOI: **https://doi.org/10.1039/d5qi01858g**.

CCDC 2441966, 2441967, 2441968, and 2441969 contain the supplementary crystallographic data for this paper.[53a–d]

Acknowledgements

The authors thank projects PID2022-136861NB-I00 and PID2023-148453NB-I00, funded by MICIU/AEI/10.13039/501100011033 and Gobierno de Aragón (Research Group E07_23R) for financial support of our research. This article is based upon work from COST Action CA22131 and LUCES Supramolecular LUminescent Chemosensors for Environmental Security, supported by COST (European Cooperation in Science and Technology). J. C. Pérez-Sánchez also thanks MICIU for a predoctoral grant (FPU21/01888). The authors would also like to acknowledge the use of Servicio General de Apoyo a la Investigación-SAI, Universidad de Zaragoza and CSIC.

References

1 R. Zhang, Q. Wang and X. Zheng, Flexible mechanochromic photonic crystals: Routes to visual sensors and their mechanical properties, *J. Mater. Chem. C*, 2018, **6**, 3182–3199.
2 M. Zhang, Y. Li, K. Gao, Z. Li, Y. Liu, Y. Liao, Y. Duan and T. Han, A turn-on mechanochromic luminescent material serving as pressure sensor and rewritable optical data storage, *Dyes Pigm.*, 2020, **173**, 107928.
3 H. Li, Y. Wang and Z. Xu, Reversible mechanochromic studies on AIE-inspired smart materials and their applications in HCHO sensing, *Dalton Trans.*, 2022, **51**, 6332–6338.
4 D. A. Davis, A. Hamilton, J. Yang, L. D. Cremar, D. Van Gough, S. L. Potisek, M. T. Ong, P. V. Braun, T. J. Martínez, S. R. White, J. S. Moore and N. R. Sottos, Force-induced activation of covalent bonds in mechanoresponsive polymeric materials, *Nature*, 2009, **459**, 68–72.
5 S. P. Anthony, Organic solid-state fluorescence: Strategies for generating switchable and tunable fluorescent materials, *ChemPlusChem*, 2012, **77**, 518–531.
6 X. Zhang, Z. Chi, Y. Zhang, S. Liu and J. Xu, Recent advances in mechanochromic luminescent metal complexes, *J. Mater. Chem. C*, 2013, **1**, 3376.
7 P. Xue, J. Ding, P. Wang and R. Lu, Recent progress in the mechanochromism of phosphorescent organic molecules and metal complexes, *J. Mater. Chem. C*, 2016, **4**, 6688–6706.
8 Y. Ai, Y. Li, M. H.-Y. Chan, G. Xiao, B. Zou and V. W.-W. Yam, Realization of distinct mechano- and piezochromic behaviors via alkoxy chain length-modulated phosphorescent properties and multidimensional self-assembly structures of dinuclear platinum(II) complexes, *J. Am. Chem. Soc.*, 2021, **143**, 10659–10667.
9 B. Xiao, S. Wu, P. Xiong, Y. Xiao, P. Shao, Z. Zhou, Y. Wang and F. Wang, Broadband near-infrared mechanoluminescence in Cr^{3+} doped $Mg_3Ga_2GeO_8$, *Chem. Eng. J.*, 2024, **498**, 155040.
10 P. Steeger, T. Theiss, D. Schwab, I. Maisuls, V. S. V. Uthayasurian, R. Schmidt, I. Kupenko, C. Sanchez-Valle, S. Michaelis de Vasconcellos, N. L. Doltsinis, C. A. Strassert and R. Bratschitsch, Reversible piezochromism of platinum(II) and palladium(II) dimers in molecular single crystals, *Nano Lett.*, 2025, **25**, 2628–2632.
11 T. Seki, Y. Takamatsu and H. Ito, A screening approach for the discovery of mechanochromic gold(I) isocyanide complexes with crystal-to-crystal phase transitions, *J. Am. Chem. Soc.*, 2016, **138**, 6252–6260.

12 T. Seki, N. Tokodai, S. Omagari, T. Nakanishi, Y. Hasegawa, T. Iwasa, T. Taketsugu and H. Ito, Luminescent mechanochromic 9-anthryl gold(I) isocyanide complex with an emission maximum at 900 nm after mechanical stimulation, *J. Am. Chem. Soc.*, 2017, **139**, 6514–6517.
13 S. Cheng, Z. Chen, Y. Yin, Y. Sun and S. Liu, Progress in mechanochromic luminescence of gold(I) complexes, *Chin. Chem. Lett.*, 2021, **32**, 3718–3732.
14 M. Montalti, A. Credi, L. Prodi and M. T. Gandolfi, *Handbook of Photochemistry*, CRC Press, 2006.
15 V. W.-W. Yam and E. C.-C. Cheng, in *Photochemistry and Photophysics of Coordination Compounds II*, ed. V. Balzani and S. Campagna, Springer, Berlin, 2007, vol. 281, pp. 269–309.
16 X. He and V. W.-W. Yam, Luminescent gold(I) complexes for chemosensing, *Coord. Chem. Rev.*, 2011, **255**, 2111–2123.
17 H. Schmidbaur and A. Schier, Aurophilic interactions as a subject of current research: An up-date, *Chem. Soc. Rev.*, 2012, **41**, 370–412.
18 T. P. Seifert, V. R. Naina, T. J. Feuerstein, N. D. Knöfel and P. W. Roesky, Molecular gold strings: Aurophilicity, luminescence and structure–property correlations, *Nanoscale*, 2020, **12**, 20065–20088.
19 R. P. Herrera and M. C. Gimeno, Main avenues in gold coordination chemistry, *Chem. Rev.*, 2021, **121**, 8311–8363.
20 J. C. Lima and L. Rodríguez, Applications of gold(I) alkynyl systems: A growing field to explore, *Chem. Soc. Rev.*, 2011, **40**, 5442.
21 M. C. Blanco, J. Cámara, M. C. Gimeno, P. G. Jones, A. Laguna, J. M. López-de-Luzuriaga, M. E. Olmos and M. D. Villacampa, Luminescent homo- and heteropolynuclear gold complexes stabilized by a unique acetylide fragment, *Organometallics*, 2012, **31**, 2597–2605.
22 M. C. Blanco, J. Cámara, M. C. Gimeno, A. Laguna, S. L. James, M. C. Lagunas and M. D. Villacampa, Synthesis of gold–silver luminescent honeycomb aggregates by both solvent-based and solvent-free methods, *Angew. Chem., Int. Ed.*, 2012, **51**, 9777–9779.
23 I. O. Koshevoy, Y.-C. Chang, Y.-A. Chen, A. J. Karttunen, E. V. Grachova, S. P. Tunik, J. Jänis, T. A. Pakkanen and P.-T. Chou, Luminescent gold(I) alkynyl clusters stabilized by flexible diphosphine ligands, *Organometallics*, 2014, **33**, 2363–2371.
24 M. C. Blanco, J. Cámara, V. Fernández-Moreira, A. Laguna and M. C. Gimeno, Gold(I), phosphanes, and alkynyls: The perfect allies in the search for luminescent compounds, *Eur. J. Inorg. Chem.*, 2018, **2018**, 2762–2767.
25 M. Pujadas and L. Rodríguez, Luminescent phosphine gold (I) alkynyl complexes. Highlights from 2010 to 2018, *Coord. Chem. Rev.*, 2020, **408**, 213179.
26 J. Gil-Rubio and J. Vicente, The coordination and supramolecular chemistry of gold metalloligands, *Chem. – Eur. J.*, 2018, **24**, 32–46.
27 B. Y.-W. Wong, H.-L. Wong, Y.-C. Wong, V. K.-M. Au, M.-Y. Chan and V. W.-W. Yam, Multi-functional bis(alkynyl) gold(III) N^C complexes with distinct mechanochromic luminescence and electroluminescence properties, *Chem. Sci.*, 2017, **8**, 6936–6946.
28 N. M. Wu, M. Ng and V. W. Yam, Photochromic benzo[*b*] phosphole alkynylgold(I) complexes with mechanochromic property to serve as multistimuli-responsive materials, *Angew. Chem., Int. Ed.*, 2019, **58**, 3027–3031.
29 N. Mirzadeh, S. H. Privér, A. J. Blake, H. Schmidbaur and S. K. Bhargava, Innovative molecular design strategies in materials science following the aurophilicity concept, *Chem. Rev.*, 2020, **120**, 7551–7591.
30 H. Ito, T. Saito, N. Oshima, N. Kitamura, S. Ishizaka, Y. Hinatsu, M. Wakeshima, M. Kato, K. Tsuge and M. Sawamura, Reversible mechanochromic luminescence of $[(C_6F_5Au)_2(\mu\text{-}1,4\text{-diisocyanobenzene})]$, *J. Am. Chem. Soc.*, 2008, **130**, 10044–10045.
31 Y.-F. Hsu, T.-W. Wu, Y.-H. Kang, C.-Y. Wu, Y.-H. Liu, S.-M. Peng, K. V. Kong and J.-S. Yang, Porous supramolecular assembly of pentiptycene-containing gold(I) complexes: Persistent excited-state aurophilicity and inclusion-induced emission enhancement, *Inorg. Chem.*, 2022, **61**, 11981–11991.
32 J. Vicente, J. Gil-Rubio, N. Barquero, P. G. Jones and D. Bautista, Synthesis of luminescent alkynyl gold metalaligands containing 2,2′-bipyridine-5-yl and 2,2′:6′,2″-terpyridine-4-yl donor groups, *Organometallics*, 2008, **27**, 646–659.
33 M. Ferrer, A. Gutiérrez, L. Rodríguez, O. Rossell, J. C. Lima, M. Font-Bardia and X. Solans, Study of the effect of the phosphane bridging chain nature on the structural and photophysical properties of a series of gold(I) ethynylpyridine complexes, *Eur. J. Inorg. Chem.*, 2008, **2008**, 2899–2909.
34 T. Zhang, Y. Hu, J. Kong, X. Meng, X. Dai and H. Song, Rational assembly and luminescence properties of 2 and 3D organometallic networks using silver(I) 4-pyridylethynide and 5-pyrimidylethynide complexes as building units, *CrystEngComm*, 2010, **12**, 3027.
35 R. Gavara, J. Llorca, J. C. Lima and L. Rodríguez, A luminescent hydrogel based on a new Au(I) complex, *Chem. Commun.*, 2012, **49**, 72–74.
36 V. Gokul, D. Devadiga and T. N. Ahipa, Pyridine based mechanochromic compounds: An overview, *Dyes Pigm.*, 2021, **195**, 109692.
37 V. W.-W. Yam and E. C.-C. Cheng, Highlights on the recent advances in gold chemistry—A photophysical perspective, *Chem. Soc. Rev.*, 2008, **37**, 1806.
38 H. Ito, M. Muromoto, S. Kurenuma, S. Ishizaka, N. Kitamura, H. Sato and T. Seki, Mechanical stimulation and solid seeding trigger single-crystal-to-single-crystal molecular domino transformations, *Nat. Commun.*, 2013, **4**, 2009.
39 H. Schmidbaur and H. G. Raubenheimer, Excimer and exciplex formation in gold(I) complexes preconditioned by aurophilic interactions, *Angew. Chem., Int. Ed.*, 2020, **59**, 14748–14771.
40 G. E. Coates and C. Parkin, 621. Gold(I) alkynyls and their co-ordination complexes, *J. Chem. Soc.*, 1962, 3220.

41 O. Ekkert, G. Kehr, R. Fröhlich and G. Erker, P–C bond activation chemistry: Evidence for 1,1-carboboration reactions proceeding with phosphorus–carbon bond cleavage, *J. Am. Chem. Soc.*, 2011, **133**, 4610–4616.
42 M. Głodek, S. Pawlędzio, A. Makal and D. Plażuk, The impact of crystal packing and aurophilic interactions on the luminescence properties in polymorphs and solvate of aroylacetylide–gold(I) complexes, *Chem. – Eur. J.*, 2019, **25**, 13131–13145.
43 T. Seki, K. Sakurada and H. Ito, Mismatched changes of the photoluminescence and crystalline structure of a mechanochromic gold(I) isocyanide complex, *Chem. Commun.*, 2015, **51**, 13933–13936.
44 A. M. Kuchison, M. O. Wolf and B. O. Patrick, Conjugated ligand-based tribochromic luminescence, *Chem. Commun.*, 2009, 7387.
45 H.-Y. Chao, W. Lu, Y. Li, M. C. W. Chan, C.-M. Che, K.-K. Cheung and N. Zhu, Organic triplet emissions of arylacetylide moieties harnessed through coordination to [Au(PCy_3)]$^+$. Effect of molecular structure upon photoluminescent properties, *J. Am. Chem. Soc.*, 2002, **124**, 14696–14706.
46 Y. Wu, Z.-H. Jiang, J.-Y. Lei, P. Shang and X.-F. Jiang, Self-assembly and mechanochromism behavior of gold(I) supramolecular cluster, *Cryst. Growth Des.*, 2023, **23**, 1477–1485.
47 R. Gautier, C. Latouche, M. Paris and F. Massuyeau, Thermochromic luminescent materials and multi-emission bands in d10 clusters, *Sci. Rep.*, 2017, **7**, 45537.
48 R. L. White-Morris, M. M. Olmstead, F. Jiang, D. S. Tinti and A. L. Balch, Remarkable variations in the luminescence of frozen solutions of [Au{C$(NHMe)_2$}$_2$](PF_6)·0.5 (acetone). Structural and spectroscopic studies of the effects of anions and solvents on gold(I) carbene complexes, *J. Am. Chem. Soc.*, 2002, **124**, 2327–2336.
49 A. J. Lees, Luminescence properties of organometallic complexes, *Chem. Rev.*, 1987, **87**, 711–743.
50 C. Jobbágy and A. Deák, Stimuli-responsive dynamic gold complexes, *Eur. J. Inorg. Chem.*, 2014, **2014**, 4434–4449.
51 S. K. Rajagopal, M. Zeller, S. Savikhin, L. V. Slipchenko and A. Wei, Rigidochromism of tetranuclear Cu(I)–pyrazolate macrocycles: Steric crowding with trifluoromethyl groups, *Chem. Commun.*, 2024, **60**, 11307–11310.
52 S. Burguera, A. Bauzá and A. Frontera, A novel approach for estimating the strength of argentophilic and aurophilic interactions using QTAIM parameters, *Phys. Chem. Chem. Phys.*, 2024, **26**, 16550–16560.
53 (*a*) CCDC 2441966: Experimental Crystal Structure Determination, 2025, DOI: **10.5517/ccdc.csd.cc2mz23t**; (*b*) CCDC 2441967: Experimental Crystal Structure Determination, 2025, DOI: **10.5517/ccdc.csd.cc2mz24v**; (*c*) CCDC 2441968: Experimental Crystal Structure Determination, 2025, DOI: **10.5517/ccdc.csd.cc2mz25w**; (*d*) CCDC 2441969: Experimental Crystal Structure Determination, 2025, DOI: **10.5517/ccdc.csd.cc2mz26x**.